ACS BIO & MED CHEM Au
AN OPEN ACCESS JOURNAL OF THE AMERICAN CHEMICAL SOCIETY

pubs.acs.org/biomedchemau
Article

The C-Terminal of $Na_V1.7$ Is Ubiquitinated by NEDD4L

Katharine M. Wright, Hanjie Jiang, Wendy Xia, Michael B. Murphy, Tatiana N. Boronina, Justin N. Nwafor, HyoJeon Kim, Akunna M. Iheanacho, P. Aitana Azurmendi, Robert N. Cole, Philip A. Cole, and Sandra B. Gabelli*

Cite This: *ACS Bio Med Chem Au* 2023, 3, 516–527
Read Online

ACCESS | Metrics & More | Article Recommendations | Supporting Information

ABSTRACT: $Na_V1.7$, the neuronal voltage-gated sodium channel isoform, plays an important role in the human body's ability to feel pain. Mutations within $Na_V1.7$ have been linked to pain-related syndromes, such as insensitivity to pain. To date, the regulation and internalization mechanisms of the $Na_V1.7$ channel are not well known at a biochemical level. In this study, we perform biochemical and biophysical analyses that establish that the HECT-type E3 ligase, NEDD4L, ubiquitinates the cytoplasmic C-terminal (CT) region of $Na_V1.7$. Through in vitro ubiquitination and mass spectrometry experiments, we identify, for the first time, the lysine residues of $Na_V1.7$ within the CT region that get ubiquitinated. Furthermore, binding studies with an NEDD4L E3 ligase modulator (ubiquitin variant) highlight the dynamic partnership between NEDD4L and $Na_V1.7$. These investigations provide a framework for understanding how NEDD4L-dependent regulation of the channel can influence the $Na_V1.7$ function.

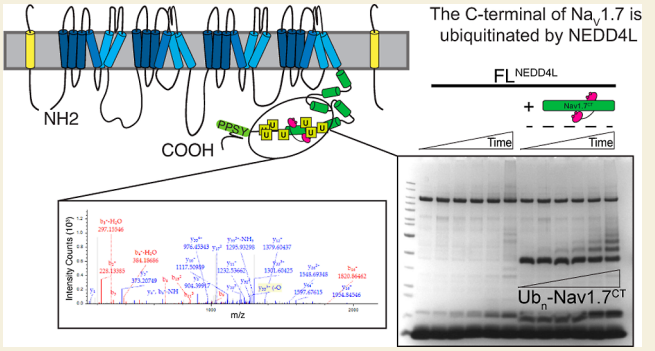

KEYWORDS: *voltage-gated sodium channel, $Na_V1.7$, SCN9A, pain, NEDD4L, NEDD4−2, E3 ligases*

INTRODUCTION

Voltage-gated sodium channels (Na_Vs) are membrane proteins that are responsible for the generation of the action potential in excitable cells by regulating the transport of sodium ions.[1−4] Of the nine Na_V isoforms that differ in tissue distribution, $Na_V1.7$ is predominantly expressed in the peripheral nervous system.[5] $Na_V1.7$ contains an alpha-pore-forming transmembrane subunit, which is associated with two auxiliary β-subunits[3] (Figure 1A, blue and yellow cylinders). Channelopathic mutations in $Na_V1.7$ have been shown to trigger pain mediation.[6−8] Specifically, loss-of-function mutations result in insensitivity to pain, and gain-of-function mutations give rise to pain hypersensitivity.[9−12]

Due to being a key regulator in pain perception, $Na_V1.7$ is a highly desired target for drug discovery.[13,14] To date, many drugs have been designed for targeting $Na_V1.7$ such as small neurotoxins, like tetrodotoxin.[15,16] Both cellular assessment and structural analyses revealed that the neurotoxins bind the extracellular alpha-pore-forming portion of the channel, persuading it into a certain state, which alters its function.[13,14,17−20] Unfortunately, these drugs lack sufficient target engagement and result in off-target effects due to the lack of selectivity since most Na_V channels share high sequence conservation of the alpha-pore-forming subunit.[21]

One alternative for therapeutic intervention is to target a region that is more isoform-selective. The Na_V cytoplasmic carboxyl-terminal (Na_V^{CT}) tail has the greatest sequence divergence among all Na_V isoforms and interacts with various proteins that regulate Na_V's membrane localization and density,[22] such as the Ca^{2+} binding protein, calmodulin (CaM), and regulatory protein NEDD4L, a HECT family ubiquitin E3 ligase (Figure 1A, green cylinders). Crystal structures of Na_V^{CT} isoforms show that the tail (residues 1773−1929 in $Na_V1.5$ and 1594−1760 in $Na_V1.4$) consists of an EF-hand-like motif (five-helical bundle) followed by a long α-helix that contains the CaM binding motif termed the IQ (isoleucine and glutamine) motif.[23−26] The CT region of $Na_V1.7$ also contains the canonical NEDD4L PY binding motif (PPSY, aa 1955−1958). The $Na_V1.7$ PY sequence has been shown to interact with domains that have two conserved tryptophan residues, also called WW domains, which are present in NEDD4L.[27] Furthermore, NEDD4L has shown specific activity via the PY motif for selective ubiquitination and regulation of $Na_V1.7$'s expression on the surface of peripheral pain-sensing neurons.[27−32] This suggests that controlling the expression of $Na_V1.7$ at the membrane by NEDD4L, in turn,

Received: May 11, 2023
Revised: September 10, 2023
Accepted: September 25, 2023
Published: October 13, 2023

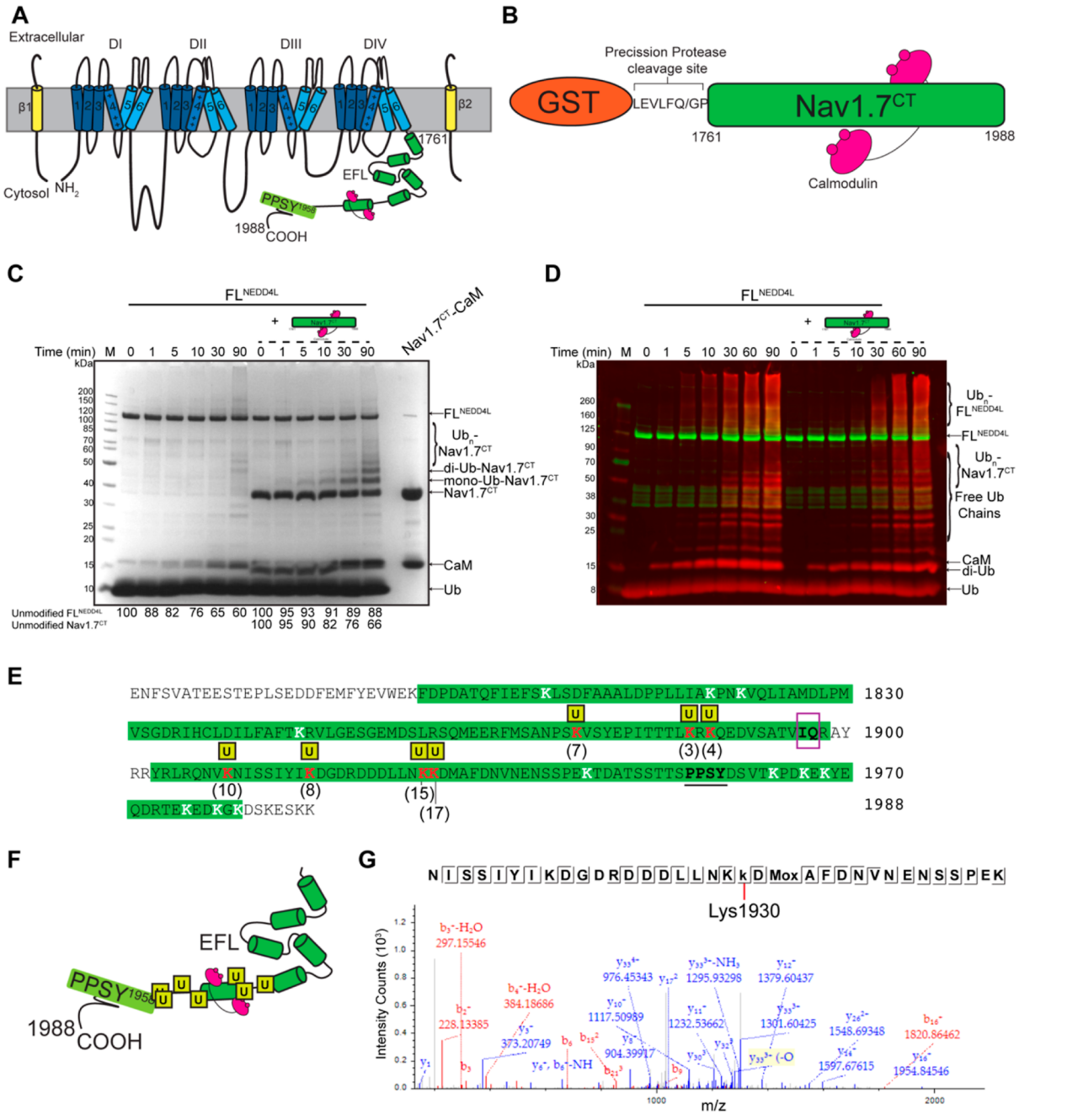

Figure 1. $Na_V1.7$ gets ubiquitinated in its C-terminal domain. (A) Scheme representation of the $Na_V1.7$ topology. Each domain and transmembrane helix are labeled accordingly. The cytoplasmic regions are shown as loops. The C-terminal of $Na_V1.7$ is shown as green cylinders representing alpha-helices as displayed in the crystallographic structures of other isoforms $Na_V1.4$ and $Na_V1.5$. The location of CaM is also highlighted in magenta. The canonical NEDD4L PY binding motif is indicated at residues 1955−1958. The two auxiliary beta subunits ($\beta1$ and $\beta2$) are shown in yellow. (B) Scheme of the GST-fusion with a precision protease cleavage sequence construct of $Na_V1.7^{CT}$spanning residues 1761−1988 (green). Coexpression was performed with full-length CaM (magenta). (C) In vitro ubiquitination time course of FL^{NEDD4L} in the absence and presence of the $Na_V1.7^{CT}$-CaM substrate. Equal amounts of sample were taken at the indicated time points and quenched with reducing loading buffer. The purified $Na_V1.7^{CT}$-CaM protein is in the last lane. Unmodified FL^{NEDD4L} and $Na_V1.7^{CT}$ substrate protein bands were quantified by a densitometry analysis as a function of time. All assays were repeated at least twice with good reproducibility ($n = 2$). Gel is stained with colloidal Coomassie Blue. (D) Fluorescent Western blot analysis of the in vitro ubiquitination assays as carried out in C using anti-ubiquitin (red) and anti-NEDD4L (green) antibodies. ($n = 2$.) (E) $Na_V1.7^{CT}$ sequence coverage after band excision from the in vitro assay. Identified peptides are highlighted in shaded green regions. Bold, red lysine residue with a yellow square above them indicate Ub-modification and the numbers in parentheses indicate total number of PSMs for each lysine identified from MS. Lysine residues detected by MS but not modified with ubiquitin are highlighted in bold, white. The IQ region is highlighted in bold and a purple box; the PY motif is bold and underlined. (F) Scheme of $Na_V1.7^{CT\text{-}CaM}$ with the ubiquitinated lysine sites labeled with yellow squares based on location. (G) Representative MS/MS spectrum and sequence coverage of the peptide containing a Ub-modification on $Na_V1.7^{CT}$-CaM Lys1930. Lower case k indicates Ub-modification and lower case m indicates an oxidized methionine.

https://doi.org/10.1021/acsbiomedchemau.3c00031
ACS Bio Med Chem Au 2023, 3, 516−527

could control the cell excitability. However, a deeper understanding of the biochemical mechanism of $Na_V1.7$ ubiquitination, regulation, and internalization is needed.

This investigation examines the targeting of $Na_V1.7$ by NEDD4L at the biochemical level. We determined the sites of ubiquitination of $Na_V1.7$ as well as the preferred ubiquitin linkage type. We also revealed the response of the $Na_V1.7$ channel to an NEDD4L modulator ubiquitin variant.

RESULTS

$Na_V1.7$ Is Ubiquitinated on Its C-Terminal Tail by NEDD4L

Sequence analysis of the full-length $Na_V1.7$ (*SCN9A*, Uniprot Q15858) protein revealed a total of 134 lysine residues. The majority of these lysine residues were located within the cytoplasmic subunits or at the interface of the cell membrane and cytoplasm. With this fact in mind and since the C-terminal (CT) of $Na_V1.7$ ($Na_V1.7^{CT}$) contains the NEDD4L binding PY motif, we designed a construct of the $Na_V1.7^{CT}$ consisting of residues 1761−1988 as a GST fusion to investigate its ubiquitination (Figure 1A,B). $Na_V1.7^{CT}$ was coexpressed and purified in the presence of CaM ($Na_V1.7^{CT}$-CaM) to increase its stability, as was previously done for other Na_V^{CT} isoforms (Figure 1B).[24,25] On sodium dodecyl sulfate-polyacrylamide gel electrophoresis (SDS-PAGE), the $Na_V1.7^{CT}$-CaM substrate ran with one band of $Na_V1.7^{CT}$ around 37 kDa and another band of CaM at 16 kDa (Figure 1C, $Na_V1.7^{CT}$-CaM lane).

To investigate possible ubiquitination of the $Na_V1.7^{CT}$-CaM substrate, in vitro ubiquitination assays were performed with full-length NEDD4L (FL^{NEDD4L}, residues 1−975) and carried out in the absence (autoubiquitination) and presence of the $Na_V1.7^{CT}$-CaM substrate. Colloidal Coomassie staining and Western blot analysis were used to visualize ubiquitination, as has been done previously with other NEDD4 E3 ligases.[33−35] Time points were determined accordingly to capture the optimal ubiquitination activity. The autoubiquitination of FL^{NEDD4L} displays a high-molecular-weight smear pattern >120 kDa above the unmodified FL^{NEDD4L} protein, which increased over 90 min (Figure 1C, lanes 2−7). The smear pattern indicates chains of multiple ubiquitin molecules (poly ubiquitination) attached to FL^{NEDD4L}. The appearance of a band at ∼16 kDa suggests free diubiquitination chains. Addition of the $Na_V1.7^{CT}$-CaM substrate showed robust substrate ubiquitination with the appearance of bands representative of different-length Ub-chains attached to the $Na_V1.7^{CT}$ band (Figure 1C, lanes 8−13). Specifically, a band representative of +9 kDa (mono-Ub) $Na_V1.7^{CT}$ appears as early as 5 min, indicating a relatively quick processing associated with the heterodimeric substrate (Figure 1C). By 90 min, there were multiple $Na_V1.7^{CT}$−Ub chain formations present including di-Ub (+18 kDa), tri-Ub (+27 kDa), and a poly ubiquitinated smear pattern (>+27 kDa) (Figure 1C). Furthermore, we observed a decrease in the unmodified $Na_V1.7^{CT}$ band as the reaction proceeded, indicating the consumption of the free protein upon ubiquitination. Importantly, $Na_V1.7^{CT}$ ubiquitination was dependent on the presence of FL^{NEDD4L} as displayed by +8 kDa bands after 1 min and strengthening of that band as well as increasing ub-chain lengths upon 5, 10 min, etc. (Figure S1, lanes 8−15). In the absence of FL^{NEDD4L}, Ub chain formation on $Na_V1.7^{CT}$ did not occur (Figure S1, lanes 2−7).

A mixture of Ub patterns of both FL^{NEDD4L} and $Na_V1.7^{CT}$ was also observed by Western blot analysis with anti-ubiquitin (red channel) and anti-NEDD4L (green channel) antibodies. Particularly, the $Na_V1.7^{CT}$ Ub pattern was mostly colocalized with the free Ub chains observed in the autoubiquitination reaction (Figures 1D and S2A, red channel). However, the area between 70 and 120 kDa at 60 and 90 min displayed increased smearing most likely attributed to $Na_V1.7^{CT}$ ubiquitination since it is not shown in its absence (Figures 1D and S1). Moreover, the Western blot highlights that the presence of the $Na_V1.7^{CT}$-CaM substrate correlates with less NEDD4L autoubiquitination (red ubiquitin and green NEDD4L signal above 120 kDa was observed as early as 10 min for FL^{NEDD4L} alone vs 30 min with $Na_V1.7^{CT}$-CaM) (Figure S2).

Importantly, unmodified CaM (band at 16 kDa) did not decrease over time, and no bands representative of CaM-ubiquitination were observed. The absence of CaM ubiquitination was confirmed by a separate in vitro assay with only CaM (Figure S3). These data revealed that the C-terminus of $Na_V1.7$ was the substrate for NEDD4L-catalyzed ubiquitination.

Ubiquitination Sites of $Na_V1.7^{CT}$ Are Proximal to the IQ Motif

To further evaluate $Na_V1.7$ ubiquitination, we determined by mass spectrometry the lysine sites on $Na_V1.7^{CT}$, which contained a Ub-modification (displayed by Gly−Gly residues at the ubiquitinated lysine residue post-tryptic digestion). Mono- and di-Ub-$Na_V1.7^{CT}$ bands were excised from SDS-PAGE at 90 min (Figure 1C) and processed by in-gel trypsin digestion and LC/MS/MS analysis. Of the 21 lysine residues within $Na_V1.7^{CT}$, the majority are located proximal to the IQ motif. MS analysis revealed 83% sequence coverage of $Na_V1.7^{CT}$ and identified 7 lysine residues with a Ub-modification (Lys1874, Lys1885, Lys1887, Lys1910, Lys1918, Lys1929, and Lys1930) (Figures 1E−G and S4). Only 4 of the 21 lysine residues were not represented in the MS coverage (Figure 1E, all identified lysines are highlighted in white). The lysine residues with the highest spectral count for Ub-modification were observed closest to the PY motif (Figure 1E,F). Furthermore, no Gly−Gly addition was observed on calmodulin in the LC/MS/MS analysis, further highlighting that only $Na_V1.7^{CT}$ was ubiquitinated.

$Na_V1.7^{CT}$ Poly Ubiquitinated Chains Formed Using Lys63 Ubiquitin Linkage

To dissect the potential for $Na_V1.7$'s cellular fate upon ubiquitination, we assessed the ubiquitin chain linkage assembled by FL^{NEDD4L} onto $Na_V1.7^{CT}$ by both MS and biochemical assays. The MS analysis was performed on the same di-Ub excised band as that in Figure 1C (90 min). Ub-modification was observed on 2 of the 7 lysine residues of ubiquitin, $Lys48^{Ub}$ and $Lys63^{Ub}$, with the latter constituting 95% of the total spectral counts (Figure 2A−C). This was expected since many of the NEDD4 family E3 ligases have been shown to facilitate Lys63-linkage.[35−37] To complement the LC/MS/MS analysis, we performed in vitro ubiquitination assays with mutated Ub proteins in the following situations: Lys48 mutated to an arginine (Ub^{K48R}), Lys63 mutated to an arginine (Ub^{K63R}) and a double mutant where both Lys48 and Lys63 are mutated to arginine residues ($Ub^{K48/63R}$). The Ub pattern of $Na_V1.7^{CT}$ in the presence of Ub^{WT} was similar to that seen in Figure 1C,D. The ubiquitination pattern of $Na_V1.7^{CT}$ in the presence of Ub^{K48R} was comparable to that of the Ub^{WT} protein (Figure 2D). In contrast, an enhancement in the ubiquitination of $Na_V1.7^{CT}$ was observed when using both Ub^{K63R} and $Ub^{K48/63R}$ (Figure 2D). The unmodified $Na_V1.7^{CT}$ protein was consumed 10−20% more by 30 min in the presence of both Ub^{K63R} mutants. We also observed more pronounced small Ub-chains, especially mono-

https://doi.org/10.1021/acsbiomedchemau.3c00031
ACS Bio Med Chem Au 2023, 3, 516−527

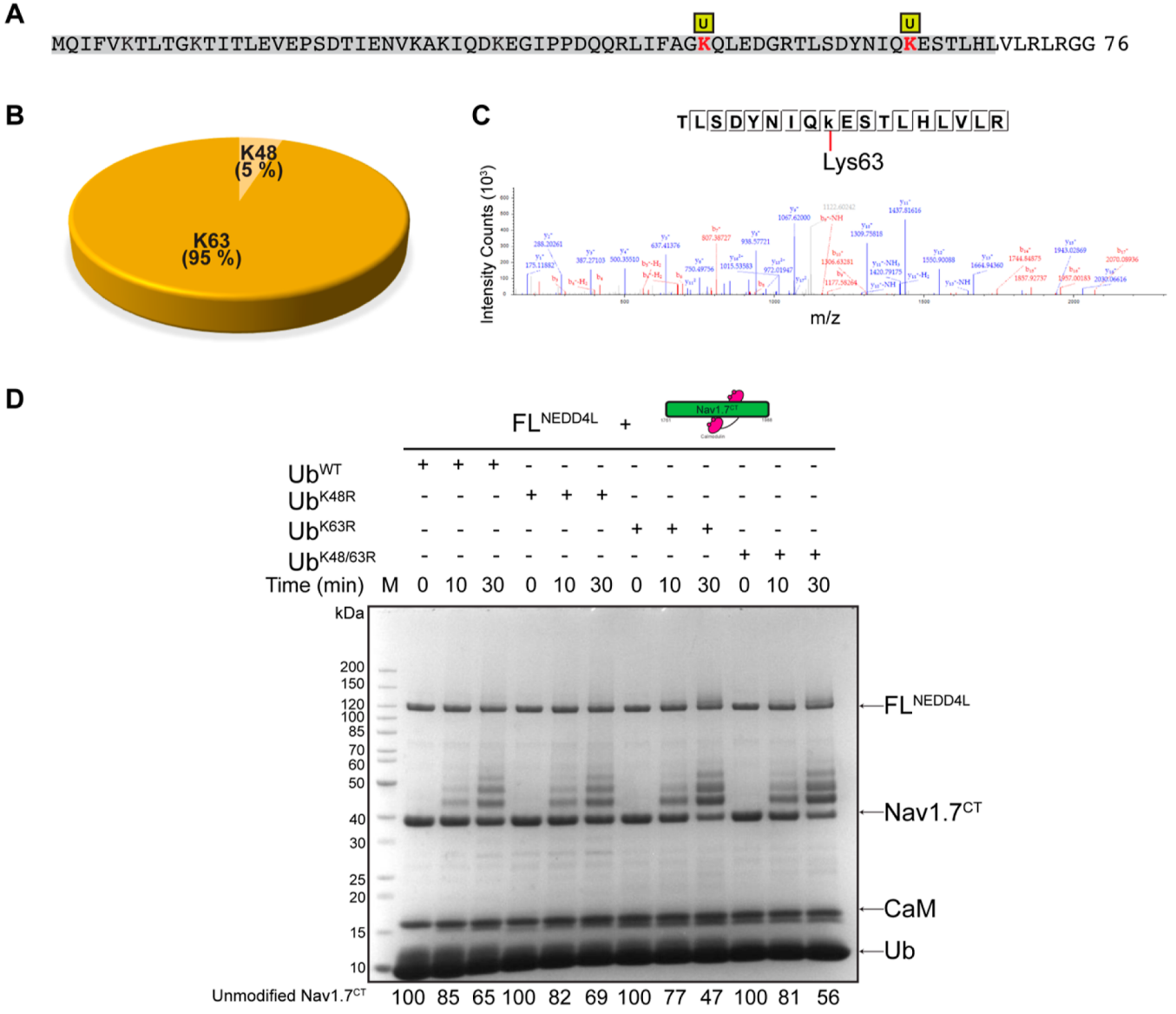

Figure 2. Lys63-linked ubiquitin chains are assembled on $Na_V1.7^{CT}$. (A) LC/MS/MS sequence coverage of ubiquitin after di-Ub-$Na_V1.7^{CT}$ band excision from the in vitro assay. Identified peptides are highlighted in shaded, boxed gray regions. Bold, red letters with a yellow square above them are the identified Lysine residues with ubiquitin chain formation. (B) Ubiquitin lysine chain linkage of $Na_V1.7^{CT}$ modified by FL^{NEDD4L} in vitro ubiquitination assay was analyzed by LC/MS/MS. The peptide spectrum matches of each ubiquitin Lysine residue seen with a Ub-modification is represented as a pie graph. (C) Representative MS/MS spectrum and sequence coverage of the peptide containing a Ub-modified Lys63. Lower case k indicates Ub-modification. (D) In vitro ubiquitination assays of $Na_V1.7^{CT}$-CaM in the presence of Ub^{WT}, Ub^{K48R}, Ub^{K63R}, or $Ub^{K48/63R}$. Samples were quenched with reducing 2× SDS-PAGE loading buffer at 0, 10, and 30 min, and the gel was stained with a colloidal Coomassie Blue stain. Unmodified $Na_V1.7^{CT}$ bands were quantified by a densitometry analysis as a function of time. All assays were repeated at least twice with good reproducibility (n = 2).

and di-Ub of $Na_V1.7^{CT}$, with ubiquitin mutants that contained K63R (Figure 2D). These results suggest that in the absence of Lys63, FL^{NEDD4L} is defective in making long Lys63-linked ubiquitin chains and easily turns to other lysine sites to produce more mono- or diubiquitinated products.

The Nav1.7^{CT}-FL^{NEDD4L} Interaction Is Dynamic

While the ubiquitination assays showed NEDD4L activity for ubiquitinating the $Na_V1.7^{CT}$-CaM complex, the biophysical properties of the interaction of these two proteins are not known. Previous studies had identified that the PY motif of the $Na_V1.7^{CT}$ (64 residues upstream from the C-terminus) bound the WW3 and WW4 domains within a truncated version of NEDD4L.[28] We designed a tandem WW3-WW4 domain construct of NEDD4L (residues aa 492−581), and the size exclusion chromatography (SEC) profiles confirmed that $Na_V1.7^{CT}$-CaM made a stable complex with WW3-4^{NEDD4L} (1.4 mL shift to the left) (Figure S5A,B). To investigate whether the binding properties of FL^{NEDD4L} would be affected, we analyzed complex formation of equal parts $Na_V1.7^{CT}$-CaM + FL^{NEDD4L} by SEC. In the chromatogram profiles, there was no additional peak or shift representative of a stable complex being formed (no significant shift in the peak representative of FL^{NEDD4L}) (Figure S5C). SDS-PAGE gel of the $Na_V1.7^{CT}$-CaM + FL^{NEDD4L} SEC elution fractions showed that the peak at 11.1 mL contained mostly FL^{NEDD4L} and impurities (Figure S5D). There was not as strong a shift as that observed with the short

https://doi.org/10.1021/acsbiomedchemau.3c00031
ACS Bio Med Chem Au 2023, 3, 516−527

tandem WW3-WW4 domain construct, indicating that $Na_V1.7^{CT}$-CaM and FL^{NEDD4L} do not form a stable complex by themselves.

To determine the binding kinetics of the interaction, we utilized surface plasmon resonance (SPR) to analyze the dynamics between $Na_V1.7^{CT}$-CaM and FL^{NEDD4L}. Initial attempts using FL^{NEDD4L} as the ligand attached to the sensor surface were unsuccessful; the full-length protein precipitated during amine coupling. Therefore, we performed all further experiments using $Na_V1.7^{CT}$-CaM as the amine-coupled ligand (Figure 3A). As a proof of concept, binding kinetics were carried out using three concentrations (6.25, 100, and 400 nM) of the injected analyte, FL^{NEDD4L}. The binding kinetic profile revealed dose-dependent binding of FL^{NEDD4L} (Figure 3B). The data were fit to a one-to-one binding model with a K_D of 11.2 nM (Figure 3B, Table S1).

Modulation of NEDD4L Activity in the Presence of Nav1.7^{CT}

Given the results from in vitro ubiquitination assays and binding studies, as well as the fact that FL^{NEDD4L} is in an autoinhibited state by itself, we hypothesized that FL^{NEDD4L} needed to be in a more active and physiological state in order to better interact with $Na_V1.7^{CT}$-CaM. Therefore, we sought to use a modulator of E3 ligase activity to better understand this relationship. One such modulator of NEDD4L activity is the ubiquitin variant that binds to the exosite of the HECT domain. The binding interaction was suggested to be important for chain processivity.[38] The designed ubiquitin variants (UbvNL.1 and.2), which bind tightly to the NEDD4L HECT exosite, have been shown to release the autoinhibition and push NEDD4L into an activated state, which could be needed for full substrate recognition and binding.[38]

In order to enhance the activity of NEDD4L, we analyzed equal parts FL^{NEDD4L} and UbvNL.1 using SEC to make a stable FL^{NEDD4L}−UbvNL.1 complex (Figure S5E,F). The SDS-PAGE gel of the FL^{NEDD4L} + UbvNL.1 SEC elution fractions showed that the peak at 11.3 mL contained both the FL^{NEDD4L} and UbvNL.1 proteins. Next, we incubated the FL^{NEDD4L}−UbvNL.1 complex with $Na_V1.7^{CT}$-CaM. The SEC profile (solid gold line) revealed there was a small shift (0.5 mL) in the peak representing FL^{NEDD4L} and the SDS-PAGE supported the fact that a stable FL^{NEDD4L}−UbvNL.1−$Na_V1.7^{CT}$-CaM complex was formed (Figure 3C,D). We further investigated the effect of UbvNL.1 by SPR. In order to keep FL^{NEDD4L} in an activated state throughout the experiment, we hypothesized that excess UbvNL.1 needed to be present throughout the SPR experiment. Previously, it had been shown that the K_D of UbvNL.1 binding to FL^{NEDD4L} was 10 nM.[38] Therefore, we performed binding kinetic experiments similar to that described above using an analyte mixture of FL^{NEDD4L} and excess UbvNL.1 (100 nM) (Figure 3E). The resulting kinetic profiles were similar to those seen with $Na_V1.7^{CT}$-CaM + FL^{NEDD4L} in the absence of UbvNL.1 (Figure 3B). However, the dissociation was slower in the presence of UbvNL.1 (0.0255 1/s; Figure 3F, Table S1). Moreover, the half-life of the $Na_V1.7^{CT}$-CaM + FL^{NEDD4L} complex with UbvNL.1 was 9 times longer than without UbvNL.1. Importantly, UbvNL.1 did not bind to $Na_V1.7^{CT}$-CaM (Figure S6).

To investigate the effect of this interaction on $Na_V1.7^{CT}$ ubiquitination, we performed an in vitro ubiquitination assay of $Na_V1.7^{CT}$-CaM, catalyzed by FL^{NEDD4L}, in the absence and presence of UbvNL.1. We detected that UbvNL.1 activated the autoubiquitination of FL^{NEDD4L}, similarly to previous reports of other NEDD4 family E3 ligases, where the unmodified FL^{NEDD4L} protein was consumed to a higher percentage at 90 min in the presence of the modulator (46% unmodified NEDD4L in the presence of UbvNL.1 vs 65% in the absence of UbvNL.1).[35] In contrast to having a reduced amount of FL^{NEDD4L} protein upon addition of UbvNL.1, the ubiquitination of $Na_V1.7^{CT}$-CaM was still quite robust but did slightly decrease (Figure 3G, 38% unmodified $Na_V1.7^{CT}$ in the absence of UbvNL.1 vs 54% unmodified $Na_V1.7^{CT}$ in the presence of UbvNL.1) (Figure 3G). Together, these data suggest that the activated form of FL^{NEDD4L} by a ubiquitin variant was preferred for binding to $Na_V1.7^{CT}$-CaM. However, since FL^{NEDD4L} becomes activated, more autoubiquitination occurs with FL^{NEDD4L} being consumed at a faster rate, leaving less enzyme to perform substrate ubiquitination.

DISCUSSION

This study delves into the molecular interaction between the voltage-gated sodium channel, $Na_V1.7$, and the HECT E3 ligase, NEDD4L. While this partnership has been identified previously by others[31,39] and highlighted functionally by Deftu et al.,[40] there were gaps in the biochemical understanding of $Na_V1.7$ regulation. We show that full-length NEDD4L catalyzes the ubiquitination of $Na_V1.7$, specifically on a selective collection of lysines within the C-terminal domain. We also show that a modulator of the NEDD4L E3 ligase activity enhances E3−substrate complex formation. Furthermore, we identified the main ubiquitin chain type of $Na_V1.7$ to be Lys63-linked ubiquitination.

Since the PY motif of $Na_V1.7$ is located on its C-terminal domain, we had hypothesized that ubiquitination sites would be located within that region. The locations of all identified Ub sites are upstream of and in close proximity to the PY motif. Sequence alignment of the nine Na_V isoforms reveals that only two of the identified ubiquitinated lysine residues are strictly conserved (Figure S7, purple star). Three of the seven identified lysine residues were mapped onto the cryoEM structure of human $Na_V1.7$ (PDB ID 7W9K), which had a portion of the visible $Na_V1.7^{CT}$ (Figure 4A).[41] One lysine is located within the EF-hand-like motif, and two are located at the beginning of the sixth α helix, which contains the IQ motif. Barring structural information on the rest of $Na_V1.7^{CT}$, the locations of other ubiquitinated lysine residues were mapped via structural alignment of the $Na_V1.4$, $Na_V1.5$, and $Na_V1.6$ channels C-terminal region (Figure 4A) and using $Na_V1.5$ in different calmodulin bound states (Figure 4B−D). Within the $Na_V1.5$ isoform (PDB ID 4OVN) structure with apo-calmodulin (no Ca^{2+} bound), one of the lysine residues, Lys1901, was located directly at the binding interface between calmodulin and the IQ motif (Figure 4B).[24] Interestingly, in both the $Na_V1.5^{CT}$-Ca^{2+}-bound CaM state (Figure 4C) and $Na_V1.5^{CT}$-apo CaM with a fibroblast growth factor 13 (FGF13) (Figure 4D), the same lysine residue was no longer obstructed.[23,42] Since our ubiquitination assays and MS showed that calmodulin does not get ubiquitinated by NEDD4L, this analysis suggests that calmodulin could be in a slightly different orientation or state to that observed with the other known isoforms, potentially affecting ubiquitination.

As mentioned, ubiquitination of the C-terminal domain had been observed before.[27] However, the previous study used a shorter version of $Na_V1.7^{CT}$, a construct that includes only the last 64 C-terminus amino acids (aa 1923−1988).[27] Our mass spectrometry data highlight that residues Lys1929 and Lys1930

https://doi.org/10.1021/acsbiomedchemau.3c00031
ACS Bio Med Chem Au 2023, 3, 516−527

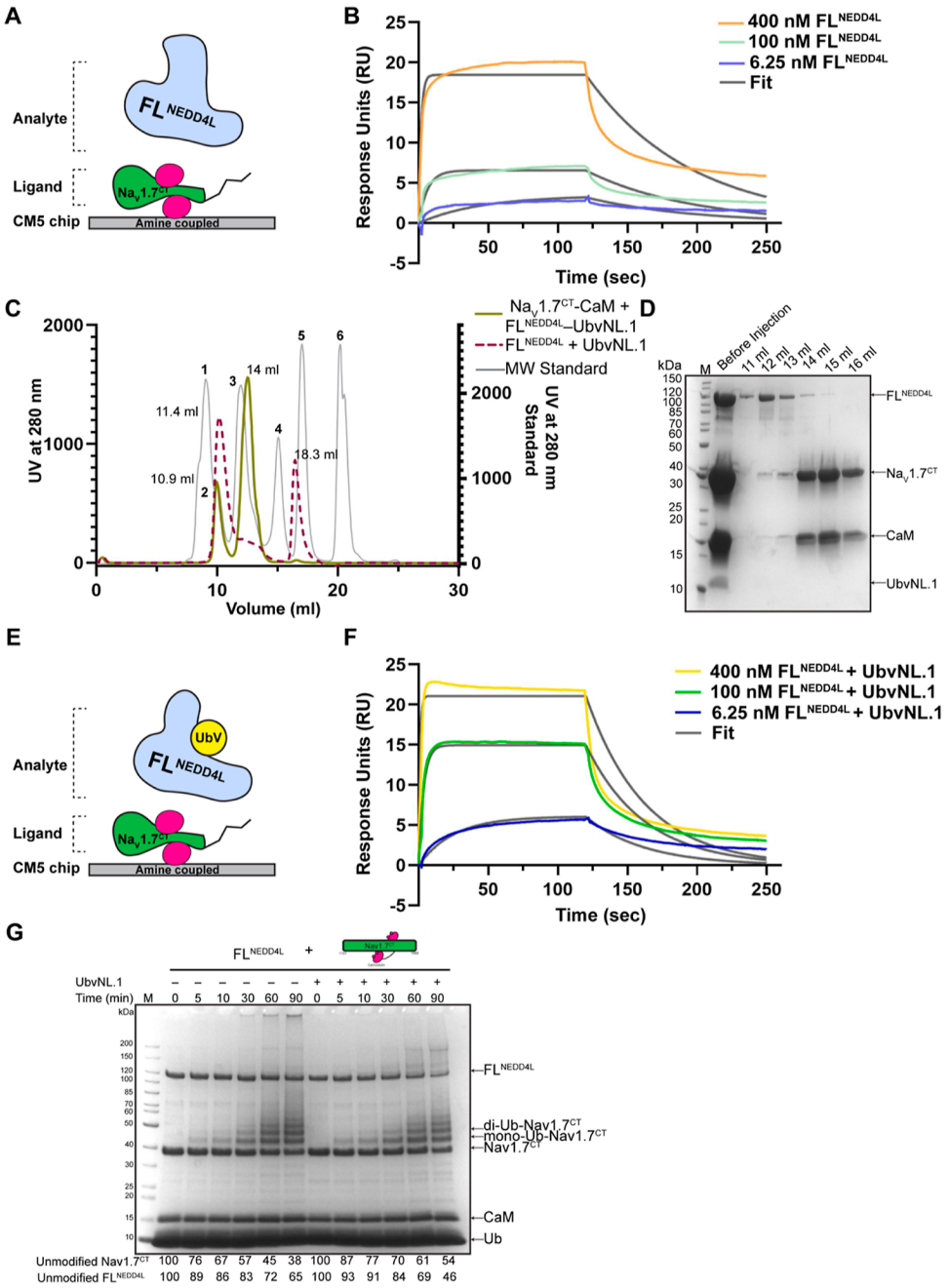

Figure 3. Binding of $Na_V1.7^{CT}$-CaM to FL^{NEDD4L} is enhanced by a ubiquitin variant. (A) Scheme of the SPR binding kinetics between $Na_V1.7^{CT}$-CaM and FL^{NEDD4L}. The ligand $Na_V1.7^{CT}$-CaM was covalently attached to a CM5 chip. The analyte, FL^{NEDD4L}, recognizes the PY motif of the $Na_V1.7^{CT}$ unstructured tail (black line). (B) FL^{NEDD4L} binding to $Na_V1.7^{CT}$-CaM was evaluated by parallel kinetics. Each binding sensorgram at 6.25, 100, and 400 nM of FL^{NEDD4L} were fit with a one-to-one binding model. $N = 2$. (C) Size exclusion chromatogram profile for $Na_V1.7^{CT}$-CaM + FL^{NEDD4L}–UbvNL.1 (solid gold line) showing $a \sim 0.5$ mL shift to the left of the FL^{NEDD4L}–UbvNL.1 peak (dashed maroon line) indicating interaction and larger molecular weight. Molecular weight standard (Biorad) is shown in gray. Bold numbers indicated each protein within the molecular weight standard: 1. thyroglobulin, 2. γ-globulin, 3. ovalbumin, 4. myoglobin, 5. vitamin B12. (D) SDS-PAGE gel showing the elution fractions from (B). The FL^{NEDD4L}–UbvNL.1-$Na_V1.7^{CT}$-CaM complex elutes are ~12 mL and excess $Na_V1.7^{CT}$-CaM elutes at 14 mL. (E) Scheme of the SPR binding kinetics as carried out in (A) with the analyte being FL^{NEDD4L} + 100 nM of ubiquitin variant, UbvNL.1. (F) FL^{NEDD4L} + UbvNL.1 binding to $Na_V1.7^{CT}$-CaM was evaluated by parallel kinetics SPR. Each binding sensorgram at 6.25, 100, and 400 nM of FL^{NEDD4L} + UbvNL.1 was fit with a one-to-one binding model. $N = 2$. (G) In vitro ubiquitination time course of $Na_V1.7^{CT}$-CaM in the absence and presence of UbvNL.1. Equal amounts of samples were taken at the indicated time points and quenched with reducing loading buffer. Unmodified $Na_V1.7^{CT}$ substrate band was quantified by a densitometry analysis as a function of time. $N = 2$.

are highly ubiquitinated in vitro by NEDD4L. Interestingly, those two lysine residues were also present in the study using the shorter 64 amino acid construct, further highlighting the importance of these two lysine residues for ubiquitination and targeting. We have also identified Lys63-linked ubiquitination to be the predominant chain type of poly ubiquitination of $Na_V1.7$. Lys63-linkage ubiquitin chains have been associated with protein sorting and transportation.[43,44] The Lys63-linked

https://doi.org/10.1021/acsbiomedchemau.3c00031
ACS Bio Med Chem Au 2023, 3, 516–527

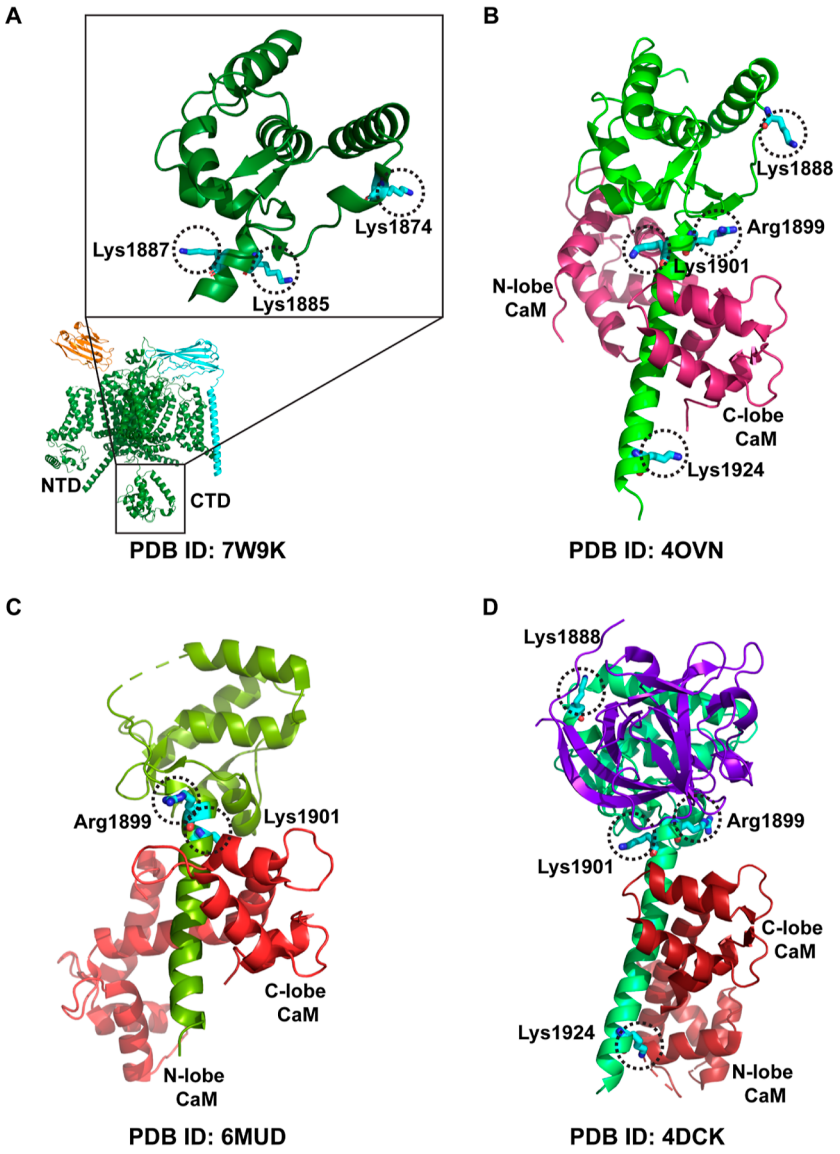

Figure 4. Mapping the locations of the ubiquitinated lysine residues of $Na_V1.7^{CT}$–CaM by sequence and structural analysis. (A) CryoEM structure of full-length human $Na_V1.7$ (PDB ID 7W9K)[41] with a zoomed in view of the C-terminal domain (CTD). $Na_V1.7$ is shown in forest green, the β1 subunit in cyan, and the β2 subunit in orange. The position of the identified lysine residues of $Na_V1.7^{CT}$-CaM are shown in cyan sticks. (B) Structure of $Na_V1.5^{CT}$ with apo-CaM (PDB ID 4OVN).[24] $Na_V1.5^{CT}$ is shown in green and apo-CaM in hot pink. The corresponding position of the identified lysine residues of $Na_V1.7^{CT}$-CaM are shown in cyan sticks. (C) Structure of $Na_V1.5^{CT}$ with calcium-bound CaM (PDB ID 6MUD)[42] structurally aligned to (A). Similarly to (A), $Na_V1.5^{CT}$ is shown in split pea and calcium-CaM in red. The corresponding positions of the identified lysine residues of $Na_V1.7^{CT}$-CaM are shown in cyan sticks. (D) Structure of $Na_V1.5^{CT}$ with apo-CaM and an FGF13 (PDB ID 4DCK)[23] structurally aligned to (A). Similarly to (A), $Na_V1.5^{CT}$ is shown in lime green, apo-CaM in dark red, and FGF13 in purple. The corresponding positions of the identified lysine residues of $Na_V1.7^{CT}$-CaM are shown in cyan sticks.

ubiquitin chain on $Na_V1.7^{CT}$ might control its membrane association and internalization. Many of the identified ubiquitinated residues lie within a region not resolved in any known Na_V structure, suggesting that they occur in dynamic, more disordered segments. While it is also possible that other cytoplasmic regions of $Na_V1.7$ can be ubiquitinated by NEDD4L, the speed at which the C-terminal region gets ubiquitinated in vitro suggests that this region may be physiologically relevant for regulating NEDD4L.

Generally, the ubiquitination of the Na_V substrate lysine residues relies on the ability of the E3 ligase to directly bind to the C-terminal PY motif or be brought into the proximity of the sodium channel. While our SEC experiments showed that the $Na_V1.7^{CT}$-CaM binds tandem NEDD4L WW domains, this interaction is not representative of the proteins in their biologically relevant states. With NEDD4L in its full-length form, a stable complex could not be formed with $Na_V1.7^{CT}$-CaM, and the binding kinetics showed a weak affinity between the two proteins. One possible explanation for these observations is that in the full-length form, the NEDD4L WW domains are not as accessible for substrate binding. However, within the ubiquitination assays, $Na_V1.7^{CT}$-CaM gets robustly ubiquitinated, suggesting that the dynamics of binding within the reaction play a role in the overall activity.

One way to explore the mechanism of the ubiquitination reaction is to investigate the effect of a modulator of NEDD4L, a ubiquitin variant molecule binding to the HECT domain exosite. To date, it has been shown that ubiquitin exosite binding

https://doi.org/10.1021/acsbiomedchemau.3c00031
ACS Bio Med Chem Au 2023, 3, 516−527

can release the autoinhibition of NEDD4 family E3 ligases, in turn activating the enzyme and pushing the enzyme into a different conformation.[33,35] Our in vitro ubiquitination assays support this. We observed an enhancement in NEDD4L autoubiquitination in the presence of UbvNL.1, the ubiquitin variant designed to bind the NEDD4L exosite with high affinity (Figure 3G). It is possible that the conformational change upon ubiquitin exosite binding results in the rearrangement of the NEDD4L WW domains, in turn making the WW domains more accessible for binding to $Na_V1.7^{CT}$-CaM. This hypothesis is supported by the increased stability between FL^{NEDD4L} and $Na_V1.7^{CT}$-CaM observed in the presence of UbvNL.1 (Figure 3E,F). However, despite the enhanced interaction, the ubiquitination of $Na_V1.7^{CT}$-CaM is slower upon the addition of UbvNL.1. Since ubiquitin exosite binding releases autoinhibition of NEDD4 family E3 ligases, it is conceivable that there could be an increase in autoubiquitination of NEDD4L, resulting in reduced unmodified enzyme present. Less NEDD4L presence would result in less ubiquitination of the $Na_V1.7^{CT}$-CaM substrate. Taken together, our data highlight a fine-tuned balance between activation of the E3 ligase and substrate targeting.

Many of the mutations associated with pain are found within the transmembrane domains of $Na_V1.7$. However, to date, there have been at least three SNP mutations that are found in the C-terminal domain of $Na_V1.7$. Two of these mutations (Trp1775Arg, Leu1831Term) are associated with congenital insensitivity to pain (CIP) and the other with neuropathic pain (Met1852Thr).[45] $Na_V1.7$ mutations related to CIP are generally loss-of-function mutations. Particularly intriguing is the Leu1831Term (Leu1831X) truncating mutation. This deletion mutation would remove a region of the C-terminal domain of the channel with three important roles in its regulation: (1) the IQ motif, which binds the regulatory protein calmodulin; (2) the NEDD4L PY binding motif; and (3) removal of all essential lysine residues used for ubiquitination. Therefore, studies of $Na_V1.7$ regulation via ubiquitination could shed light on pain phenotypes and provide a promising direction for the therapeutic targeting of these channels.

METHODS

Plasmids and Reagents

Human ubiquitin-activating enzyme UBE1, human ubiquitin-conjugating enzyme UbcH5c, and the constructs for Ub^{K48R}, Ub^{K63R}, and $Ub^{K48/63R}$ were a gift from Dr. Cynthia Wolberger, Johns Hopkins University. The E1 and E2 enzymes were purified as described before.[46]

Protein Coexpression and Purification of GST-Tagged $Na_V1.7^{CT}$–CaM

cDNA sequence coding for $Na_V1.7^{CT}$ (aa 1761–1988, Q15858) was selected by aligning the sequences of *Homo sapiens* $Na_V1.7$, $Na_V1.5^{CT}$,[24] and $Na_V1.4^{CT}$[25] and choosing the equivalent region to the one known to crystallize. The selected $Na_V1.7^{CT}$ sequence was then subcloned into the pGEX6p-1 expression vector, which rendered a clone with N-Terminal GST with a PreScission protease sequence (Genscript). DNA sequence coding for calmodulin (CaM; aa 1–149, P0DP23) was subcloned into a pET24b expression vector.[24] Both plasmids were cotransformed into BL21-CodonPlus RIL *E. coli* cells. The transformed cells were cultured in LB medium, supplemented with 100 μg/mL carbenicillin, 50 μg/mL kanamycin, and 25 μg/mL chloramphenicol, at 37 °C to reach the optimal density (OD_{600} = 0.8) on an 8 L scale. Protein production was induced with 0.5 mM isopropyl thiogalactoside (IPTG) and grown overnight at 18 °C for 20 h. Cells were harvested at 4000*g*, and the cell pellets were frozen at −80 °C.

Upon thawing, the cells were resuspended in lysis buffer (1X phosphate-buffered saline (PBS) pH 7.4, 300 mM NaCl and 5 mM DTT) supplemented with 1% Triton X-100. Cells were lysed using a microfluidizer (Microfluidics Corporation; model 110 Y), and the lysates were clarified at 11,000 x rpm for 1 h. The supernatants were incubated overnight with 3 mL of pre-equilibrated GSH-agarose. Following overnight incubation, the cell lysate was loaded onto a gravity flow column. The beads with bound protein were washed with 1X PBS, pH 7.5, 100 mM NaCl, and 1 mM DTT. The desired GST-tagged $Na_V1.7^{CT}$–CaM complex was eluted using 1X PBS, 1 mM DTT, and 10 mM reduced glutathione at pH 8.0. The eluted fractions were combined and dialyzed against a buffer consisting of 25 mM TRIS HCl, pH 8.0, 50 mM NaCl, and 1 mM DTT. The protein was also treated with the PreScission protease at 4 °C overnight to cleave the GST tag. Afterward, the mixture of GST and cleaved proteins were loaded onto a Source Q anion exchange column (Cytiva). Elution was performed using the buffer 25 mM TRIS HCl, pH 8, and 1 mM DTT and a step gradient of 50–500 mM NaCl. Fractions were analyzed by SDS-PAGE and assessed for >98% purity. For in vitro and binding assays, the purified $Na_V1.7^{CT}$–CaM protein was concentrated to ∼2–4 mg/mL, flash frozen, and stored at −80 °C.

Protein Expression and Purification of GST-Tagged FL^{NEDD4L} and $WW34^{NEDD4L}$

The pcDNA3.1(+) plasmid with the full-length NEDD4L human sequence (amino acids 1–975; Q96PU5) was purchased from Addgene. DNA sequence coding for the FL^{NEDD4L} (aa 1–975) and $WW34^{NEDD4L}$ (aa 492–581) proteins were subcloned into the pGEX6p-1 expression vector and transformed into BL21-CodonPlus RIL *E. coli* cells. The transformed cells were cultured in LB medium, supplemented with 100 μg/mL carbenicillin and 25 μg/mL chloramphenicol, at 37 °C to reach the optimal density (OD_{600} = 0.8) on an 8 L scale. Protein production was induced with 0.5 mM IPTG and grown overnight at 18 °C for 20 h. Cells were harvested at 4000*g*, and the cell pellets were frozen at −80 °C.

Upon thawing, the cells were resuspended in lysis buffer [25 mM *N*-(2-hydroxyethyl)piperazine-N′-ethanesulfonic acid (HEPES) pH 7.5, 300 mM NaCl, 1 mM DTT] supplemented with 0.5% Triton X-100, 1 mM phenylmethylsulfonyl fluoride (PMSF), and 1× Roche cocktail protease inhibitors. Cells were lysed using a microfluidizer (Microfluidics Corporation; model 110 Y), and the lysate was clarified at 11,000 × rpm for 1 h. The supernatant was loaded onto 3 mL of GSH-agarose (pre-equilibrated with lysis buffer) using a gravity flow column, followed by washing with 25 mM HEPES, pH 7.5, 300 mM NaCl, 1 mM DTT, and 0.1% Triton X-100. The desired GST-tagged FL^{NEDD4L} protein was eluted using 25 mM HEPES, 300 mM NaCl, 1 mM DTT, and 20 mM reduced glutathione at pH 8.0. The eluted fractions were combined and dialyzed against a buffer consisting of 25 mM HEPES, pH 7.5, 50 mM NaCl, and 1 mM TCEP. The protein was also treated with the PreScission protease at 4 °C overnight to cleave the GST tag. Afterward, the mixture of GST and cleaved proteins were loaded onto a Source Q anion exchange column (Cytiva). Elution was performed using the buffer 25 mM HEPES, pH 7.5, 1 mM TCEP, and a step gradient of 50–500 mM NaCl. Fractions were analyzed by SDS-PAGE and assessed for >98% purity. For in vitro and binding assays, the purified FL^{NEDD4L} was concentrated to ∼2–4 mg/mL, flash-frozen, and stored at −80 °C.

Wild-Type and Lysine Mutant Ubiquitin Protein Expression and Purification

DNA sequences coding for human wild-type (WT) and lysine mutant (K48R, K63R, and K48/63R) ubiquitin proteins were subcloned into pET3a and transformed into BL21(DE3) *E. coli* cells. The transformed cells were cultured in LB medium on a 2 L scale at 37 °C until an OD_{600} = 0.6. Protein production was initiated by the addition of 0.5 mM IPTG at 16 °C for 16 h. The cells were resuspended in 50 mM TRIS at pH 7.6, 10 mM $MgCl_2$, 0.01% Triton X-100, and 1 mM PMSF and lysed via a microfluidizer. The ubiquitin supernatants were collected, placed on ice, and precipitated by dropwise addition of 70% v/v solution of perchloric acid while stirring. Precipitation was stopped once reaching

https://doi.org/10.1021/acsbiomedchemau.3c00031
ACS Bio Med Chem Au 2023, 3, 516–527

pH 4−5, and centrifugation was performed at 11,000 × rpm to separate out the precipitate. The clarified supernatant was dialyzed against 50 mM ammonium sulfate at pH 4.5 overnight at 4 °C and then loaded onto a Source S cation exchange column (Cytiva). Elution was performed using a linear gradient with 500 mM NaCl in 50 mM ammonium sulfate, pH 4.5. Relevant fractions were analyzed by SDS-PAGE for 98% purity, pooled, and dialyzed into 20 mM HEPES, pH 7.5, 50 mM NaCl, and 0.5 mM DTT. For ubiquitination assays, purified WT and lysine mutant ubiquitin proteins were concentrated to ∼2−4 mg/mL.

Protein Expression and Purification of Ubiquitin Variant UbvNL.1

The UbvNL.1 cDNA was synthesized through Integrated DNA Technology and subcloned into a pGEX6p-2 plasmid vector and then transformed into BL-21 Codon Plus RIL *E. coli* cells. The *E. coli* cells were cultured in LB medium at 37 °C on a 2 L scale, and protein production was initiated with 0.5 mM IPTG and grown overnight at 16 °C for 20 h. Collected cells were resuspended in lysis buffer (25 mM HEPES, pH 7.5, 250 mM NaCl, 1 mM DTT) supplemented with 1× cocktail protease inhibitor (Thermo Fisher) and 1 mM PMSF. Cells were lysed using a microfluidizer, and the lysate was clarified at 11,000 × rpm for 1 h. The supernatant was loaded onto 3 mL of pre-equilibrated GSH-agarose using a gravity flow column, followed by washing with 25 mM HEPES, pH 7.5, 250 mM NaCl, 1 mM DTT, and 0.1% Triton X-100. The desired GST-tagged ubiquitin variant UbvNL.1 was eluted using 25 mM HEPES, 300 mM NaCl, 1 mM DTT, and 50 mM reduced glutathione at pH 8.0. The eluted fractions were combined and dialyzed against a buffer consisting of 25 mM HEPES, pH 7.5, 250 mM NaCl, and 1 mM DTT. The protein was treated with the PreScission protease at 4 °C overnight to cleave the GST tag. Afterward, SEC with a Superdex 75 Increase 10/300 GL column (Cytiva) was used to further purify the protein in the running buffer 25 mM HEPES, pH 7.5, 250 mM NaCl, and 1 mM DTT. Purified fractions (purity > 90%) were combined, concentrated, and stored at −80 °C.

Purification of Calmodulin

Calmodulin (CaM) was coexpressed with an N-terminal GST-tagged C-Terminus domain of $Na_V1.5$ ($Na_V1.5^{CT}$) in BL21(DE3) cells and purified using a GST Sepharose column described by Srinivasan et al. with minor modifications.[47] Briefly, *E. coli* cells cotransformed with the DNA sequence coding calmodulin (CaM; aa 1−149, P0DP23), $Na_V1.5^{CT}$ were cultured in LB medium at 37 °C on a 2 L scale, and protein production was initiated with 1 mM IPTG and grown overnight at 18 °C for 20 h. Collected cells were resuspended in lysis buffer (25 mM Tris−HCl, pH 8, 500 mM NaCl, 5 mM DTT, 1% Triton X-100) with 1 mM PMSF. The cells were lysed via a microfluidizer, and the lysate was isolated by centrifugation at 11,000 rpm for 1 h. After 0.22 μM filtration, the lysate was incubated with 3 mL of 1× PBS buffer equilibrated GST resin, made to flow through a gravity column, and washed with 30 mL of 1× PBS with an additional 100 mM NaCl. A sample of the wash fraction was analyzed by SDS-PAGE and judged to be >95% free CaM, which was concentrated and stored at −80 °C.

Size Exclusion Chromatography

SEC was performed to assess the formation of multiple complexes by using purified proteins. For Figure S5A, $Na_V1.7^{CT-}$CaM and $WW34^{NEDD4L}$ were mixed in a 1:2 molar ratio, incubated overnight at 4 °C, and run using 25 mM HEPES, pH 7.5, 200 mM NaCl, and 1 mM DTT on a Superdex 75 Increase 10/300 GL column (Cytiva, 29148721). The $WW34^{NEDD4L}$ protein was run using 25 mM HEPES, pH 7.5, 240 mM NaCl, and 1 mM TCEP on a Superdex 75 10/300 GL column (Cytiva). For Figure S5B, $Na_V1.7^{CT-}$CaM and FL^{NEDD4L} were mixed in a 1:1 molar ratio, incubated overnight at 4 °C, and run using 25 mM HEPES, pH 7.5, 200 mM NaCl, and 1 mM DTT on a Superdex 200 Increase 10/300 GL column (Cytiva, 28990944). For Figure S5C, FL^{NEDD4L} and UbvNL.1 were mixed in a 1:1.5 molar ratio, incubated overnight at 4 °C, and run using 25 mM HEPES, pH 7.5, 200 mM NaCl, and 1 mM TCEP on a Superdex 200 Increase 10/300 GL column (Cytiva, 28990944). For Figure 3, $Na_V1.7^{CT-}$CaM and FL^{NEDD4L}−UbvNL.1 were mixed in a 5:1 molar ratio, incubated overnight at 4 °C, and run using 25 mM HEPES, pH 7.5, 200 mM NaCl, and 1 mM TCEP on a Superdex 200 Increase 10/300 GL column (Cytiva, 28990944). The Biorad gel filtration marker (1511901) was used as the molecular weight standard. Chromatograms were exported as Excel files, and analysis and plotting were configured in GraphPad Prism (GraphPad Software, Inc.).

SPR Affinity Measurements

$Na_V1.7^{CT-CaM}$, FL^{NEDD4L}, and UbvNL.1 binding experiments were performed at 25 °C using a Biacore 8 K and 1S+ SPR instrument (Cytiva, Inc.). Approximately ∼200−280 response units of $Na_V1.7^{CT-CaM}$ were captured in channels 1−8, using amine coupling. Parallel binding kinetics was performed by injecting increasing concentrations (6.25, 100, and 400 nM) of purified FL^{NEDD4L}, using channels 1−4. Parallel binding kinetics with UbvNL.1 were performed by injecting increasing concentrations (6.25, 100, and 400 nM) of purified FL^{NEDD4L} + 100 nM UbvNL.1, using channels 5−8. Binding responses for kinetic analysis were both blank-subtracted and reference-subtracted.[48] Both binding curves were fit with a 1:1 binding model by using Biacore Insight evaluation software. The UbvNL.1 control was performed similarly, with 100 nM UbvNL.1 made to flow over the amine-coupled $Na_V1.7^{CT-CaM}$.

In Vitro Ubiquitination Assays

In vitro ubiquitination assays were performed in a 1 mL microcentrifuge tube at a total volume of 30 μL containing 50 nM E1, 3 μM E2 (UbcH5c), 50 μM ubiquitin (Ub), 2.5 μM FL^{NEDD4L} protein, 5−10 μM $Na_V1.7^{CT-CaM}$ substrate with 40 mM Tris−HCl, pH 7.5, 50 mM NaCl, 0.5 mM TCEP, 5 mM ATP, and 5 mM $MgCl_2$. The reactions were initiated by the addition of E1 and carried out at 30 °C. The reactions were quenched at the indicated time points with the addition of 2× SDS-PAGE reducing loading buffer. The reaction samples were then boiled for 5 min at 97 °C and loaded onto a 12% SDS-PAGE gel along with a molecular weight marker (Thermo Scientific, PageRuler Unstained Protein Ladder, 3 μL). The gels were analyzed using colloidal Coomassie Blue staining following the manufacturer's protocol. Briefly, the SDS-PAGE gel was first primed for staining by washing with a 50% ethanol/10% acetic acid solution for 10 min, followed by washing with distilled water for 5 min. After priming, 100 mL of a staining solution containing 10% ammonium sulfate, 2% phosphoric acid 85%, 5% CBB G-250, and 20% ethanol was added to the SDS-PAGE and incubated overnight. After sufficient destaining, the unmodified E3 protein bands, highlighted underneath each gel, were quantified by using ImageJ densitometry and normalized to the zero time points.

Western Blots

Protein samples from the in vitro ubiquitination assays were loaded on a 12% SDS-PAGE gel and transferred to a poly(vinylidene difluoride) membrane using a Power Blotter dry-blotting system (Thermo Fisher Scientific) for 10 min. The membranes were blocked with Intercept (TBS) Blocking buffer (LiCOR) for 1 h at room temperature. Anti-NEDD4L (Cell Signaling #4013 1:2000 in 5% BSA) was diluted in 0.05% TBS-Tween-20 (TBS/T) and added to the membrane and incubated at 4 °C overnight. After this, antiubiquitin (SCBT #sc-8017, 1:2000 dilution) was added to the 0.05% TBS-Tween-20-primary antibody solution and incubated at room temperature for 1 h. The membranes were then washed with TBS/T 4 × 5 min and probed with IRDye antimouse 800 (ubiquitin) and antirabbit 680 (NEDD4L) secondary antibodies at 1:10,000 dilution. The bands were detected on a LiCOR Odyssey CLx. All assays were repeated on at least two independent occasions, with replicates revealing results similar to the data in the figures.

Ubiquitin Site Mapping by Mass Spectrometry

Ubiquitination sites of $Na_V1.7^{CT-CaM}$ were identified by tandem mass spectrometry (MS/MS). Proteins were separated via SDS-PAGE and visualized with colloidal Coomassie blue staining. $Na_V1.7^{CT-CaM}$-Ub bands were excised, cut into 1 mm × 1 mm pieces, and dehydrated with methanol for 5 min. All samples were reduced with DTT, alkylated with

https://doi.org/10.1021/acsbiomedchemau.3c00031
ACS Bio Med Chem Au 2023, 3, 516−527

methyl methanethiolsulfonate (MMTS), and digested with trypsin (Promega, 12.5 ng/μL in 40 μL of 50 mM TEAB at 37 °C overnight[49]). Tryptic peptides were extracted with 50% acetonitrile and 0.1% TFA, dried, reconstituted with 150 μL of 0.1% TFA in water, acidified, and desalted on u-HLB Oasis plates (Waters). Desalted peptides were analyzed by nano-LC/MS/MS on an Orbitrap Fusion Lumos (Thermo Fisher) interfaced with an EASY LC 1000 system (Thermo Fisher). Peptides were separated using reverse-phase chromatography at 300 nL/min, on 75 μm × 150 mm ProntoSIL-120−5-C18H columns of 3 μm, 120 Å (BISCHOFF) using 2−90% acetonitrile/0.1% FA gradient (solvent B) over 86 min 4 A: 2 to 8% B by 1 min; 8 to 25% B by 61 min, 25 to 45% B by 81 min; and 100% acetonitrile by 86 min. Eluting peptides were sprayed into an Orbitrap Fusion Lumos mass spectrometer through a 1 μm emitter tip (New Objective) at 2.6 kV. Survey scans (Full MS) were acquired between 370 and 1800 m/z at a resolution 120 K, AGC target 4×10^5, max inject time 60 ms, using data-dependent acquisition of the top 15 ions with dynamic exclusion of 15 s. Precursor ions, individually isolated within 0.7 m/z, were fragmented with higher energy collision dissociation (HCD) set to 32 and analyzed at a resolution of 30 K, ACG-predicted max inject time 118 ms, and 3 cycles.

Peptide and fragment ion masses were extracted from the raw mass spectra in Proteome Discoverer (PD) software (v2.3, Thermo-Scientific) and searched using PEAKS Studio Xpro (v. X, Bioinformatics Solution Inc.) and Mascot (v2.6.2, Matrix Science, London, UK) against three databases containing the human Sodium channel protein type 9 subunit alpha (Uniprot: Q15858) and *H. sapiens* WT ubiquitin C (Uniprot: L8B196). Specific search parameters were as follows: precursor s/n 1.5, mass tolerance 5 ppm, fragment mass tolerance 0.01 m/z, Lys ubiquitination (GlyGly), Met oxidation, Cys carbamidomethylation, and Asn/Gln deamidation as variable modifications. Mascot files were sent to PD2.3 for PSM validation with Percolator. All MS/MS spectra assigned to modified $Na_V1.7^{CT-CaM}$ or ubiquitin peptides were manually inspected, and the relative abundances of the ubiquitin chain linkages and sites were determined using spectral counting.

■ ASSOCIATED CONTENT

Data Availability Statement

All mass spectrometry raw data have been deposited at iProX Consortium and are publicly available as of the date of publication (name of the data source or link).

Supporting Information

The Supporting Information is available free of charge at https://pubs.acs.org/doi/10.1021/acsbiomedchemau.3c00031.

SPR binding kinetics data of FL^{NEDD4L} for $Na_V1.7^{CT}$-CaM in the absence and presence of UbvNL.1, in vitro ubiquitination assay of $Na_V1.7^{CT}$-CaM in the absence and presence of FL^{NEDD4L}, fluorescent Western blot detection of $Na_V1.7^{CT}$ in vitro ubiquitination, in vitro ubiquitination assay of FL^{NEDD4L} in the absence and presence of CaM, representative MS/MS spectra and sequence coverage of the Gly−Gly-modified $Na_V1.7^{CT}$ peptides, protein−protein complex formation detected by SEC, SPR binding sensorgram of excess UbvNL.1 to $Na_V1.7^{CT}$-CaM, and sequence alignment of the CT region of the nine Na_V isoforms (PDF)

■ AUTHOR INFORMATION

Corresponding Author

Sandra B. Gabelli − *Department of Biophysics and Biophysical Chemistry, The Johns Hopkins School of Medicine, Baltimore, Maryland 21205, United States; Department of Medicine, The Johns Hopkins University School of Medicine, Baltimore, Maryland 21205, United States; Department of Oncology, The Johns Hopkins University School of Medicine, Baltimore, Maryland 21287, United States;* Present Address: present address Discovery Chemistry, MRL, Merck Please check: & Co, Inc. West Point, PA, 19846, USA; orcid.org/0000-0003-1205-5204; Email: sandra.gabelli@merck.com

Authors

Katharine M. Wright − *Department of Biophysics and Biophysical Chemistry, The Johns Hopkins School of Medicine, Baltimore, Maryland 21205, United States;* Present Address: present address Discovery Chemistry, MRL, Merck Please check: & Co, Inc. West Point, PA, 19846, USA

Hanjie Jiang − *Division of Genetics, Department of Medicine, Brigham and Women's Hospital, Boston, Massachusetts 02115, United States; Department of Biological Chemistry and Molecular Pharmacology, Harvard Medical School, Boston, Massachusetts 02115, United States; Department of Pharmacology and Molecular Sciences, Johns Hopkins School of Medicine, Baltimore, Maryland 21205, United States*

Wendy Xia − *Department of Biophysics and Biophysical Chemistry, The Johns Hopkins School of Medicine, Baltimore, Maryland 21205, United States*

Michael B. Murphy − *Cytiva, Marlborough, Massachusetts 01752, United States*

Tatiana N. Boronina − *Mass Spectrometry and Proteomics Facility, Department of Biological Chemistry, Johns Hopkins University School of Medicine, Baltimore, Maryland 21205, United States*

Justin N. Nwafor − *Department of Biophysics and Biophysical Chemistry, The Johns Hopkins School of Medicine, Baltimore, Maryland 21205, United States*

HyoJeon Kim − *Division of Genetics, Department of Medicine, Brigham and Women's Hospital, Boston, Massachusetts 02115, United States; Department of Biological Chemistry and Molecular Pharmacology, Harvard Medical School, Boston, Massachusetts 02115, United States;* orcid.org/0009-0001-2658-3510

Akunna M. Iheanacho − *Department of Biophysics and Biophysical Chemistry, The Johns Hopkins School of Medicine, Baltimore, Maryland 21205, United States; Department of Physiology, The Johns Hopkins School of Medicine, Baltimore, Maryland 21205, United States*

P. Aitana Azurmendi − *Department of Biophysics and Biophysical Chemistry, The Johns Hopkins School of Medicine, Baltimore, Maryland 21205, United States*

Robert N. Cole − *Mass Spectrometry and Proteomics Facility, Department of Biological Chemistry, Johns Hopkins University School of Medicine, Baltimore, Maryland 21205, United States*

Philip A. Cole − *Division of Genetics, Department of Medicine, Brigham and Women's Hospital, Boston, Massachusetts 02115, United States; Department of Biological Chemistry and Molecular Pharmacology, Harvard Medical School, Boston, Massachusetts 02115, United States;* orcid.org/0000-0001-6873-7824

Complete contact information is available at: https://pubs.acs.org/10.1021/acsbiomedchemau.3c00031

Author Contributions

Conceptualization was performed by S.B.G.; methodology was executed by K.M.W., H.J., W.X., M.M., T.N.B., J.N.N., H.K.,

A.M.I., P.A.A., R.C., P.A.C., and S.B.G.; validation was carried out by K.W., H.J., and T.B.; formal analysis was accomplished by K.W., H.J., and T.B.; investigation resources were obtained by S.B.G. and P.A.C.; writing and editing were done by K.M.W. and S.B.G.; all authors edited and approved the final version of the manuscript. CRediT: **Katharine M Wright** conceptualization, formal analysis, supervision, validation, writing-original draft, writing-review & editing; **Hanjie Jiang** investigation, methodology, writing-review & editing; **Wendy Xia** investigation, writing-review & editing; **Michael B Murphy** investigation, methodology, writing-review & editing; **Tatiana N Boronina** investigation, methodology, writing-review & editing; **Justin N Nwafor** investigation, methodology, writing-review & editing; **HyoJeon Kim** investigation; **Akunna M Iheanacho** investigation, methodology, writing-review & editing; **P. Aitana Azurmendi** investigation; **Robert N. Cole** investigation, methodology, supervision, writing-review & editing; **Philip A Cole** funding acquisition, supervision, validation, writing-review & editing; **Sandra B. Gabelli** conceptualization, funding acquisition, project administration, writing-review & editing.

Funding

This work was funded by NIH NHLBI HL128743 and NIGMS GM62437 and NCI CA74305. J.N.N. was supported by NIH R25 GM109441 and by the Vivien Thomas Scholars Initiative at the Johns Hopkins University.

Notes

The authors declare no competing financial interest.

■ ACKNOWLEDGMENTS

This study was supported in part by NIH Grant CA74305. The mass spectrometry analysis was carried out at the Johns Hopkins University School of Medicine Mass Spectrometry and Proteomics Facility, which is supported by the Sidney Kimmel Comprehensive Cancer Center (NCI grant 2P30 CA006973) and Hopkins Conte NIH/NIDDK Digestive Diseases Basic and Translational Research Core Center (P30 DK089502). Human ubiquitin-activating enzyme UBE1, human ubiquitin-conjugating enzyme UbcH5c, and the constructs for Ub^{K48R}, Ub^{K63R} were a gift from Dr. Cynthia Wolberger, JHU. The authors thank Xiangbin Zhang for the technical suggestions.

■ REFERENCES

(1) Hodgkin, A. L.; Huxley, A. F. A quantitative description of membrane current and its application to conduction and excitation in nerve. *J. Physiol.* **1952**, *117*, 500−544.

(2) Fozzard, H. A.; Hanck, D. A. Structure and function of voltage-dependent sodium channels: comparison of brain II and cardiac isoforms. *Physiol. Rev.* **1996**, *76*, 887−926.

(3) Catterall, W. A. From ionic currents to molecular mechanisms: the structure and function of voltage-gated sodium channels. *Neuron* **2000**, *26*, 13−25.

(4) Hille, B. Ionic channels in excitable membranes. Current problems and biophysical approaches. *Biophys. J.* **1978**, *22*, 283−294.

(5) Goldin, A. L.; Barchi, R. L.; Caldwell, J. H.; Hofmann, F.; Howe, J. R.; Hunter, J. C.; Kallen, R. G.; Mandel, G.; Meisler, M. H.; Netter, Y. B.; Noda, M.; Tamkun, M. M.; Waxman, S. G.; Wood, J. N.; Catterall, W. A. Nomenclature of voltage-gated sodium channels. *Neuron* **2000**, *28*, 365−368.

(6) Yang, Y.; Wang, Y.; Li, S.; Xu, Z.; Li, H.; Ma, L.; Fan, J.; Bu, D.; Liu, B.; Fan, Z.; Wu, G.; Jin, J.; Ding, B.; Zhu, X.; Shen, Y. Mutations in SCN9A, encoding a sodium channel alpha subunit, in patients with primary erythermalgia. *J. Med. Genet.* **2004**, *41*, 171−174.

(7) Cox, J. J.; Reimann, F.; Nicholas, A. K.; Thornton, G.; Roberts, E.; Springell, K.; Karbani, G.; Jafri, H.; Mannan, J.; Raashid, Y.; Al-Gazali, L.; Hamamy, H.; Valente, E. M.; Gorman, S.; Williams, R.; McHale, D. P.; Wood, J. N.; Gribble, F. M.; Woods, C. G. An SCN9A channelopathy causes congenital inability to experience pain. *Nature* **2006**, *444*, 894−898.

(8) Cai, S.; Moutal, A.; Yu, J.; Chew, L. A.; Isensee, J.; Chawla, R.; Gomez, K.; Luo, S.; Zhou, Y.; Chefdeville, A.; Madura, C.; Perez-Miller, S.; Bellampalli, S. S.; Dorame, A.; Scott, D. D.; Francois-Moutal, L.; Shan, Z.; Woodward, T.; Gokhale, V.; Hohmann, A. G.; Vanderah, T. W.; Patek, M.; Khanna, M.; Hucho, T.; Khanna, R. Selective targeting of NaV1.7 via inhibition of the CRMP2-Ubc9 interaction reduces pain in rodents. *Sci. Transl. Med.* **2021**, *13*, No. eabh1314.

(9) Dib-Hajj, S. D.; Rush, A. M.; Cummins, T. R.; Hisama, F. M.; Novella, S.; Tyrrell, L.; Marshall, L.; Waxman, S. G. Gain-of-function mutation in Nav1.7 in familial erythromelalgia induces bursting of sensory neurons. *Brain* **2005**, *128*, 1847−1854.

(10) Cummins, T. R.; Dib-Hajj, S. D.; Waxman, S. G. Electrophysiological properties of mutant Nav1.7 sodium channels in a painful inherited neuropathy. *J. Neurosci.* **2004**, *24*, 8232−8236.

(11) Nassar, M. A.; Stirling, L. C.; Forlani, G.; Baker, M. D.; Matthews, E. A.; Dickenson, A. H.; Wood, J. N. Nociceptor-specific gene deletion reveals a major role for Nav1.7 (PN1) in acute and inflammatory pain. *Proc. Natl. Acad. Sci. U.S.A.* **2004**, *101*, 12706−12711.

(12) Wisedchaisri, G.; Gamal El-Din, T. M.; Zheng, N.; Catterall, W. A. Structural basis for severe pain caused by mutations in the S4-S5 linkers of voltage-gated sodium channel Na(V)1.7. *Proc. Natl. Acad. Sci. U.S.A.* **2023**, *120* (14), No. e2219624120.

(13) Ahuja, S.; Mukund, S.; Deng, L.; Khakh, K.; Chang, E.; Ho, H.; Shriver, S.; Young, C.; Lin, S.; Johnson, J. P., Jr.; Wu, P.; Li, J.; Coons, M.; Tam, C.; Brillantes, B.; Sampang, H.; Mortara, K.; Bowman, K. K.; Clark, K. R.; Estevez, A.; Xie, Z.; Verschoof, H.; Grimwood, M.; Dehnhardt, C.; Andrez, J. C.; Focken, T.; Sutherlin, D. P.; Safina, B. S.; Starovasnik, M. A.; Ortwine, D. F.; Franke, Y.; Cohen, C. J.; Hackos, D. H.; Koth, C. M.; Payandeh, J. Structural basis of Nav1.7 inhibition by an isoform-selective small-molecule antagonist. *Science* **2015**, *350*, aac5464.

(14) Payandeh, J.; Hackos, D. H. Selective Ligands and Drug Discovery Targeting the Voltage-Gated Sodium Channel Nav1.7. *Handb. Exp. Pharmacol.* **2018**, *246*, 271−306.

(15) Mulcahy, J. V.; Pajouhesh, H.; Beckley, J. T.; Delwig, A.; Du Bois, J.; Hunter, J. C. Challenges and Opportunities for Therapeutics Targeting the Voltage-Gated Sodium Channel Isoform NaV1.7. *J. Med. Chem.* **2019**, *62*, 8695−8710.

(16) Goncalves, T. C.; Benoit, E.; Partiseti, M.; Servent, D. The NaV1.7 Channel Subtype as an Antinociceptive Target for Spider Toxins in Adult Dorsal Root Ganglia Neurons. *Front. Pharmacol* **2018**, *9*, 1000.

(17) Catterall, W. A.; Cestele, S.; Yarov-Yarovoy, V.; Yu, F. H.; Konoki, K.; Scheuer, T. Voltage-gated ion channels and gating modifier toxins. *Toxicon* **2007**, *49*, 124−141.

(18) Shen, H.; Liu, D.; Wu, K.; Lei, J.; Yan, N. Structures of human Nav1.7 channel in complex with auxiliary subunits and animal toxins. *Science* **2019**, *363*, 1303−1308.

(19) Zhang, F.; Xu, X.; Li, T.; Liu, Z. Shellfish toxins targeting voltage-gated sodium channels. *Mar. Drugs* **2013**, *11*, 4698−4723.

(20) Xu, H.; Li, T.; Rohou, A.; Arthur, C. P.; Tzakoniati, F.; Wong, E.; Estevez, A.; Kugel, C.; Franke, Y.; Chen, J.; Ciferri, C.; Hackos, D. H.; Koth, C. M.; Payandeh, J. Structural Basis of Nav1.7 Inhibition by a Gating-Modifier Spider Toxin. *Cell* **2019**, *176*, 702−715.e14.

(21) Hagen, N. A.; Cantin, L.; Constant, J.; Haller, T.; Blaise, G.; Ong-Lam, M.; du Souich, P.; Korz, W.; Lapointe, B. Tetrodotoxin for Moderate to Severe Cancer-Related Pain: A Multicentre, Randomized, Double-Blind, Placebo-Controlled, Parallel-Design Trial. *Pain Res. Manag.* **2017**, *2017*, 7212713.

(22) Catterall, W. A. Signaling complexes of voltage-gated sodium and calcium channels. *Neurosci. Lett.* **2010**, *486*, 107−116.

(23) Wang, C.; Chung, B. C.; Yan, H.; Lee, S. Y.; Pitt, G. S. Crystal structure of the ternary complex of a NaV C-terminal domain, a fibroblast growth factor homologous factor, and calmodulin. *Structure* **2012**, *20*, 1167−1176.

(24) Gabelli, S. B.; Boto, A.; Kuhns, V. H.; Bianchet, M. A.; Farinelli, F.; Aripirala, S.; Yoder, J.; Jakoncic, J.; Tomaselli, G. F.; Amzel, L. M. Regulation of the NaV1.5 cytoplasmic domain by calmodulin. *Nat. Commun.* **2014**, *5*, 5126.
(25) Yoder, J. B.; Ben-Johny, M.; Farinelli, F.; Srinivasan, L.; Shoemaker, S. R.; Tomaselli, G. F.; Gabelli, S. B.; Amzel, L. M. Ca(2+)-dependent regulation of sodium channels NaV1.4 and NaV1.5 is controlled by the post-IQ motif. *Nat. Commun.* **2019**, *10*, 1514.
(26) Wang, C.; Chung, B. C.; Yan, H.; Wang, H. G.; Lee, S. Y.; Pitt, G. S. Structural analyses of Ca(2)(+)/CaM interaction with NaV channel C-termini reveal mechanisms of calcium-dependent regulation. *Nat. Commun.* **2014**, *5*, 4896.
(27) Fotia, A. B.; Ekberg, J.; Adams, D. J.; Cook, D. I.; Poronnik, P.; Kumar, S. Regulation of neuronal voltage-gated sodium channels by the ubiquitin-protein ligases Nedd4 and Nedd4−2. *J. Biol. Chem.* **2004**, *279*, 28930−28935.
(28) Laedermann, C. J.; Cachemaille, M.; Kirschmann, G.; Pertin, M.; Gosselin, R. D.; Chang, I.; Albesa, M.; Towne, C.; Schneider, B. L.; Kellenberger, S.; Abriel, H.; Decosterd, I. Dysregulation of voltage-gated sodium channels by ubiquitin ligase NEDD4−2 in neuropathic pain. *J. Clin. Invest.* **2013**, *123*, 3002−3013.
(29) Staub, O.; Abriel, H.; Plant, P.; Ishikawa, T.; Kanelis, V.; Saleki, R.; Horisberger, J. D.; Schild, L.; Rotin, D. Regulation of the epithelial Na+ channel by Nedd4 and ubiquitination. *Kidney Int.* **2000**, *57*, 809−815.
(30) Cachemaille, M.; Laedermann, C. J.; Pertin, M.; Abriel, H.; Gosselin, R. D.; Decosterd, I. Neuronal expression of the ubiquitin ligase Nedd4−2 in rat dorsal root ganglia: modulation in the spared nerve injury model of neuropathic pain. *Neuroscience* **2012**, *227*, 370−380.
(31) Laedermann, C. J.; Decosterd, I.; Abriel, H. Ubiquitylation of voltage-gated sodium channels. *Handb. Exp. Pharmacol.* **2014**, *221*, 231−250.
(32) Ekberg, J. A.; Boase, N. A.; Rychkov, G.; Manning, J.; Poronnik, P.; Kumar, S. Nedd4−2 (NEDD4L) controls intracellular Na(+)-mediated activity of voltage-gated sodium channels in primary cortical neurons. *Biochem. J.* **2014**, *457*, 27−31.
(33) Chen, Z.; Jiang, H.; Xu, W.; Li, X.; Dempsey, D. R.; Zhang, X.; Devreotes, P.; Wolberger, C.; Amzel, L. M.; Gabelli, S. B.; Cole, P. A. A Tunable Brake for HECT Ubiquitin Ligases. *Mol. Cell* **2017**, *66*, 345−357.e6.
(34) Wang, Z.; Liu, Z.; Chen, X.; Li, J.; Yao, W.; Huang, S.; Gu, A.; Lei, Q. Y.; Mao, Y.; Wen, W. A multi-lock inhibitory mechanism for fine-tuning enzyme activities of the HECT family E3 ligases. *Nat. Commun.* **2019**, *10*, 3162.
(35) Jiang, H.; Thomas, S. N.; Chen, Z.; Chiang, C. Y.; Cole, P. A. Comparative analysis of the catalytic regulation of NEDD4−1 and WWP2 ubiquitin ligases. *J. Biol. Chem.* **2019**, *294*, 17421−17436.
(36) Tao, M.; Scacheri, P. C.; Marinis, J. M.; Harhaj, E. W.; Matesic, L. E.; Abbott, D. W. ITCH K63-ubiquitinates the NOD2 binding protein, RIP2, to influence inflammatory signaling pathways. *Curr. Biol.* **2009**, *19*, 1255−1263.
(37) Ma, M.; Yang, W.; Cai, Z.; Wang, P.; Li, H.; Mi, R.; Jiang, Y.; Xie, Z.; Sui, P.; Wu, Y.; Shen, H. SMAD-specific E3 ubiquitin ligase 2 promotes angiogenesis by facilitating PTX3 degradation in MSCs from patients with ankylosing spondylitis. *Stem Cell.* **2021**, *39*, 581−599.
(38) Zhang, W.; Wu, K. P.; Sartori, M. A.; Kamadurai, H. B.; Ordureau, A.; Jiang, C.; Mercredi, P. Y.; Murchie, R.; Hu, J.; Persaud, A.; Mukherjee, M.; Li, N.; Doye, A.; Walker, J. R.; Sheng, Y.; Hao, Z.; Li, Y.; Brown, K. R.; Lemichez, E.; Chen, J.; Tong, Y.; Harper, J. W.; Moffat, J.; Rotin, D.; Schulman, B. A.; Sidhu, S. S. System-Wide Modulation of HECT E3 Ligases with Selective Ubiquitin Variant Probes. *Mol. Cell* **2016**, *62*, 121−136.
(39) Abriel, H.; Kamynina, E.; Horisberger, J. D.; Staub, O. Regulation of the cardiac voltage-gated Na+ channel (H1) by the ubiquitin-protein ligase Nedd4. *FEBS Lett.* **2000**, *466*, 377−380.
(40) Deftu, A. F.; Chu Sin Chung, P.; Laedermann, C. J.; Gillet, L.; Pertin, M.; Kirschmann, G.; Decosterd, I. The Antidiabetic Drug Metformin Regulates Voltage-Gated Sodium Channel Na(V)1.7 via the Ubiquitin-Ligase NEDD4−2. *eNeuro* **2022**, *9*, No. ENEURO.0409-21.2022.
(41) Huang, G.; Liu, D.; Wang, W.; Wu, Q.; Chen, J.; Pan, X.; Shen, H.; Yan, N. High-resolution structures of human Nav1.7 reveal gating modulation through α-π helical transition of S6IV. *Cell Rep.* **2022**, *39*, 110735.
(42) Gardill, B. R.; Rivera-Acevedo, R. E.; Tung, C. C.; Van Petegem, F. Crystal structures of Ca(2+)-calmodulin bound to Na(V) C-terminal regions suggest role for EF-hand domain in binding and inactivation. *Proc. Natl. Acad. Sci. U.S.A.* **2019**, *116*, 10763−10772.
(43) Yau, R.; Rape, M. The increasing complexity of the ubiquitin code. *Nat. Cell Biol.* **2016**, *18*, 579−586.
(44) Lauwers, E.; Jacob, C.; Andre, B. K63-linked ubiquitin chains as a specific signal for protein sorting into the multivesicular body pathway. *J. Cell Biol.* **2009**, *185*, 493−502.
(45) Emery, E. C.; Habib, A. M.; Cox, J. J.; Nicholas, A. K.; Gribble, F. M.; Woods, C. G.; Reimann, F. Novel SCN9A mutations underlying extreme pain phenotypes: unexpected electrophysiological and clinical phenotype correlations. *J. Neurosci.* **2015**, *35*, 7674−7681.
(46) Raasi, S.; Pickart, C. M. Rad23 ubiquitin-associated domains (UBA) inhibit 26 S proteasome-catalyzed proteolysis by sequestering lysine 48-linked polyubiquitin chains. *J. Biol. Chem.* **2003**, *278*, 8951−8959.
(47) Srinivasan, L.; Alzogaray, V.; Selvakumar, D.; Nathan, S.; Yoder, J. B.; Wright, K. M.; Klinke, S.; Nwafor, J. N.; Labanda, M. S.; Goldbaum, F. A.; Schon, A.; Freire, E.; Tomaselli, G. F.; Amzel, L. M.; Ben-Johny, M.; Gabelli, S. B. Development of high-affinity nanobodies specific for Na(V)1.4 and Na(V)1.5 voltage-gated sodium channel isoforms. *J. Biol. Chem.* **2022**, *298*, 101763.
(48) Myszka, D. G. Improving biosensor analysis. *J. Mol. Recognit.* **1999**, *12*, 279−284.
(49) Shevchenko, A. W.; Wilm, M.; Vorm, O.; Mann, M. Mass Spectrometric Sequencing of Proteins from Silver-Stained Polyacrylamide Gels. *Anal. Chem.* **1996**, *68*, 850−858.

https://doi.org/10.1021/acsbiomedchemau.3c00031
ACS Bio Med Chem Au 2023, 3, 516−527